25. N. Sato, L. Meijer, L. Skaltsounis, P. Greengard, A. H. Brivanlou, *Nat. Med.* **10**, 55 (2004).
26. I. Chambers *et al.*, *Cell* **113**, 643 (2003).
27. H. Zaehres *et al.*, *Stem Cells* **23**, 299 (2005).
28. P. Deb-Rinker, A. Ly, A. Jezierski, M. Sikorska, P. R. Walker, *J. Biol. Chem.* **280**, 6257 (2005).
29. We thank J. Zucker, B. Haas, and H. Chipperfield for technical support; N. Benvenisty and R. Eiges for the *Rex1*-GFP reporter construct, the *Rex1*-GFP transgenic BJ fibroblasts, and for critical reading of this manuscript; A. Meissner and R. Jaenisch for the lentiviral vector; and A. Aggarwal and C. Morton for karyotyping services. C.C. is a Damon Runyon Fellow. This work was supported in part by the Naomi Berrie Diabetes Center and the Rx Foundation and was reviewed and approved by the standing committees on animal research, stem cell research, and human subjects research in the Faculty of Arts and Sciences at Harvard University.

Supporting Online Material
www.sciencemag.org/cgi/content/full/309/5739/1369/DC1
Materials and Methods
Figs. S1 to S3
Tables S1 to S4

22 June 2005; accepted 1 August 2005
10.1126/science.1116447

Spatial Coordination of Spindle Assembly by Chromosome-Mediated Signaling Gradients

Maïwen Caudron,[1] Gertrude Bunt,[2] Philippe Bastiaens,[1]* Eric Karsenti[1]*

During cell division, chromosomes are distributed to daughter cells by the mitotic spindle. This system requires spatial cues to reproducibly self-organize. We report that such cues are provided by chromosome-mediated interaction gradients between the small guanosine triphosphatase (GTPase) Ran and importin-β. This produces activity gradients that determine the spatial distribution of microtubule nucleation and stabilization around chromosomes and that are essential for the self-organization of microtubules into a bipolar spindle.

Two models have been proposed to explain how microtubules (MTs) become organized into a bipolar spindle. In the "search-and-capture" model, the dynamic plus ends of MTs nucleated at centrosomes are randomly captured and stabilized at the kinetochores on the chromosomes (*1*). However, in numerous systems, spindle assembly occurs in the absence of extrachromosomal nucleating centers (*2*–*5*). Therefore, another model has been proposed in which chromatin changes the state of the mitotic cytoplasm in its surrounding area and promotes spindle assembly through a self-organization process (*6*, *7*). Experiments have confirmed part of this model. It has been shown that chromatin beads incubated in frog egg extracts promote MT nucleation in their vicinity (*8*) and stabilize MTs at great distances (*9*), which results in the self-organization of a bipolar spindle. Central to this model is the small guanosine triphosphatase (GTPase) Ran, which exists in a guanosine triphosphate (GTP)–bound

[1]Cell Biology and Biophysics Department, European Molecular Biology Laboratory (EMBL), EMBL, 69117 Heidelberg, Germany. [2]Max-Planck-Institut für Experimentelle Medizin, 37075 Göttingen, Germany.

*To whom correspondence should be addressed. E-mail: karsenti@embl-heidelberg.de (E.K.) and bastiaen@embl-heidelberg.de (P.B.)

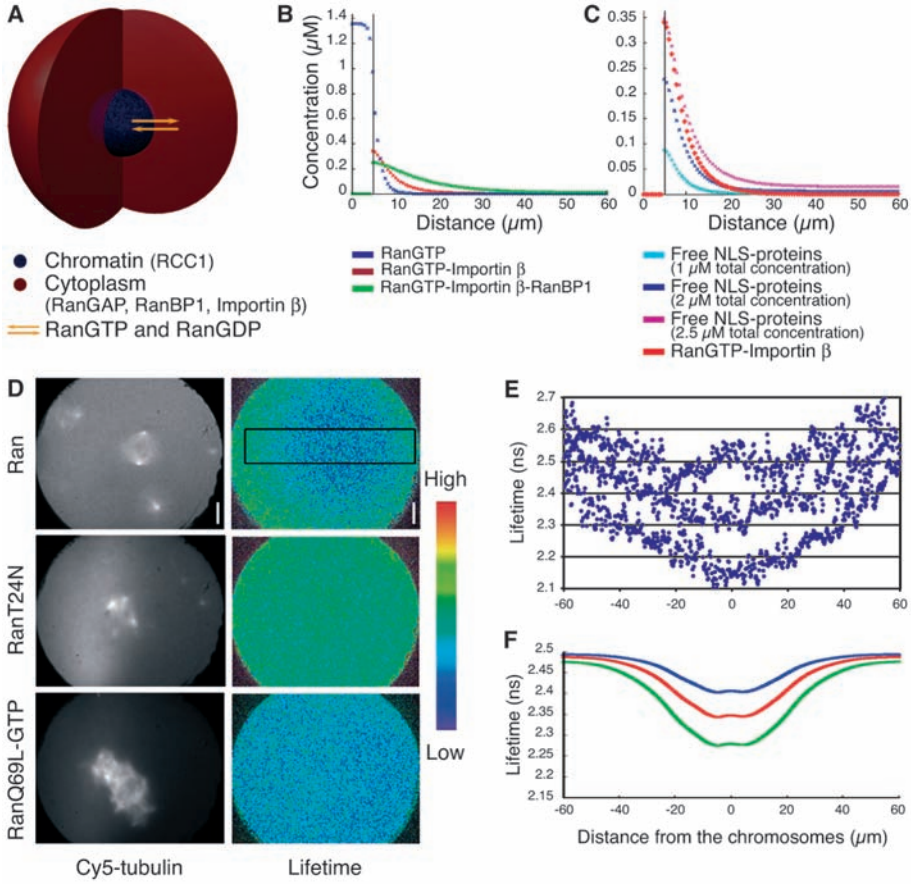

Fig. 1. (**A**) The Ran system was modeled in a spherical space where RanGTP and RanGDP diffuse between chromatin (5 μm radius) and the cytoplasm (60 μm radius), whereas other species are restricted to their own compartments. (**B**) Calculated spatial distribution of RanGTP species concentrations at steady state. Vertical black line, interface between chromatin (left side) and cytoplasm (right side). (**C**) Calculated spatial distribution of free NLS-protein concentration relative to the RanGTP–importin-β distribution. (**D**) Spatial distribution of Alexa 488–Ran lifetime (top right) around a mitotic spindle (top left) (*22*). Blue to green reflects a decreasing interaction between RanGTP and importin-β (color bar). The same experiment, done in the presence of inactive (RanT24N, middle) or active Ran (RanQ69L-GTP, bottom), results in global fluorescence lifetime changes. Scale bars, 15 μm. (**E**) Lifetime profiles were measured around sperm nuclei in different mitotic extracts inside the window (D). (**F**) Theoretical lifetime profiles were computed from relative concentrations of species having a fluorescence lifetime of 2.1 ns or 2.5 ns and ratios of 1:1 (blue), 2:1 (red), and 4:1 (green). Chromatin induces a slight increase in fluorescence lifetime at the center because of the local high Ran-RCC1 complex concentration (2.5-ns fluorescence lifetime). This was observed experimentally to variable extents [top curve in (E)].

active form (RanGTP) close to chromosomes and in a guanosine diphosphate (GDP)-bound inactive form (RanGDP) in the cytoplasm. These two states occur because of the high activity of Ran-GTPase–activating protein (RanGAP), which is cytoplasmic, and a Ran–guanosine nucleotide exchange factor (RanGEF or RCC1) that is localized on chromosomes (*10*–*14*). A short-range RanGTP gradient has indeed been visualized around chromosomes in metaphase *Xenopus* egg extracts and cells (*14*, *15*). However, such a short-range RanGTP gradient cannot explain the observation of long-range effects of chromatin on asymmetric growth of MTs (*9*, *16*). Moreover, free RanGTP does not affect MT nucleation and dynamics directly but rather through the release of MT regulatory NLS-proteins from karyopherins (*13*, *14*). It is thus the resulting spatial distribution of free nuclear localization signal–containing (NLS) proteins that determines where MT nucleation and plus end stabilization occur and that coordinates the spatial organization of MTs into a bipolar spindle.

To examine the formation of RanGTP-dependent downstream effector gradients around metaphase chromosomes, we first modeled the Ran system as a reaction-diffusion process in a spherical space (Fig. 1A). Because of the sequestration of RCC1 on chromosomes and the predominantly homogeneous distribution of RanGAP in the cytoplasm, two different regions harbor different sets of reactions. The central area corresponds to the space occupied by the chromatin that contains RCC1. It is surrounded by the cytoplasm, containing RanGAP and its associated protein RanBP1, as well as the karyopherin importin-β. Ran diffuses in the whole space and forms complexes with RCC1, RanBP1, and importin-β (Fig. 1A) (*17*). The system evolves rapidly and independently of the initial conditions toward a steady state, to generate a steep gradient of free RanGTP around chromosomes (Fig. 1B), which matches the RanGTP gradient measured in *Xenopus* egg extracts (*15*). However, this system also generates RanGTP-dependent long-range gradients that are more physiologically relevant: the RanGTP–importin-β and RanGTP–importin-β–RanBP1 gradients (Fig. 1B). These are the gradients that actually determine both short- and long-range chromatin effects by spatially controlling the release of NLS-proteins that affect MT nucleation and dynamics. Indeed, free NLS-proteins exist only where importin-β is in a complex with RanGTP (Fig. 1C) (*17*). Such long-range gradients exist because the stable RanGTP–importin-β complex prevents RanGAP-induced GTP hydrolysis and thus diffuses away from chromatin (*18*), until dissociation is induced by RanBP1 and importin α binding (*19*, *20*). The RanGTP–importin-β–RanBP1 gradient extends further and builds on the RanGTP–importin-β gradient just as the latter does on the local production of RanGTP around chromosomes.

We investigated directly the span of the RanGTP–importin-β interaction using fluorescence lifetime imaging microscopy (FLIM) (*21*). To measure the interaction between RanGTP and importin-β, fluorescence resonance energy transfer (FRET) between Alexa 488–tagged Ran and Cy3-labeled importin-β was imaged by the decrease in fluorescence lifetime of the Alexa 488 donor (*22*). Extended gradients of RanGTP–importin-β interaction were observed around assembling spindles in metaphase *Xenopus* egg extracts

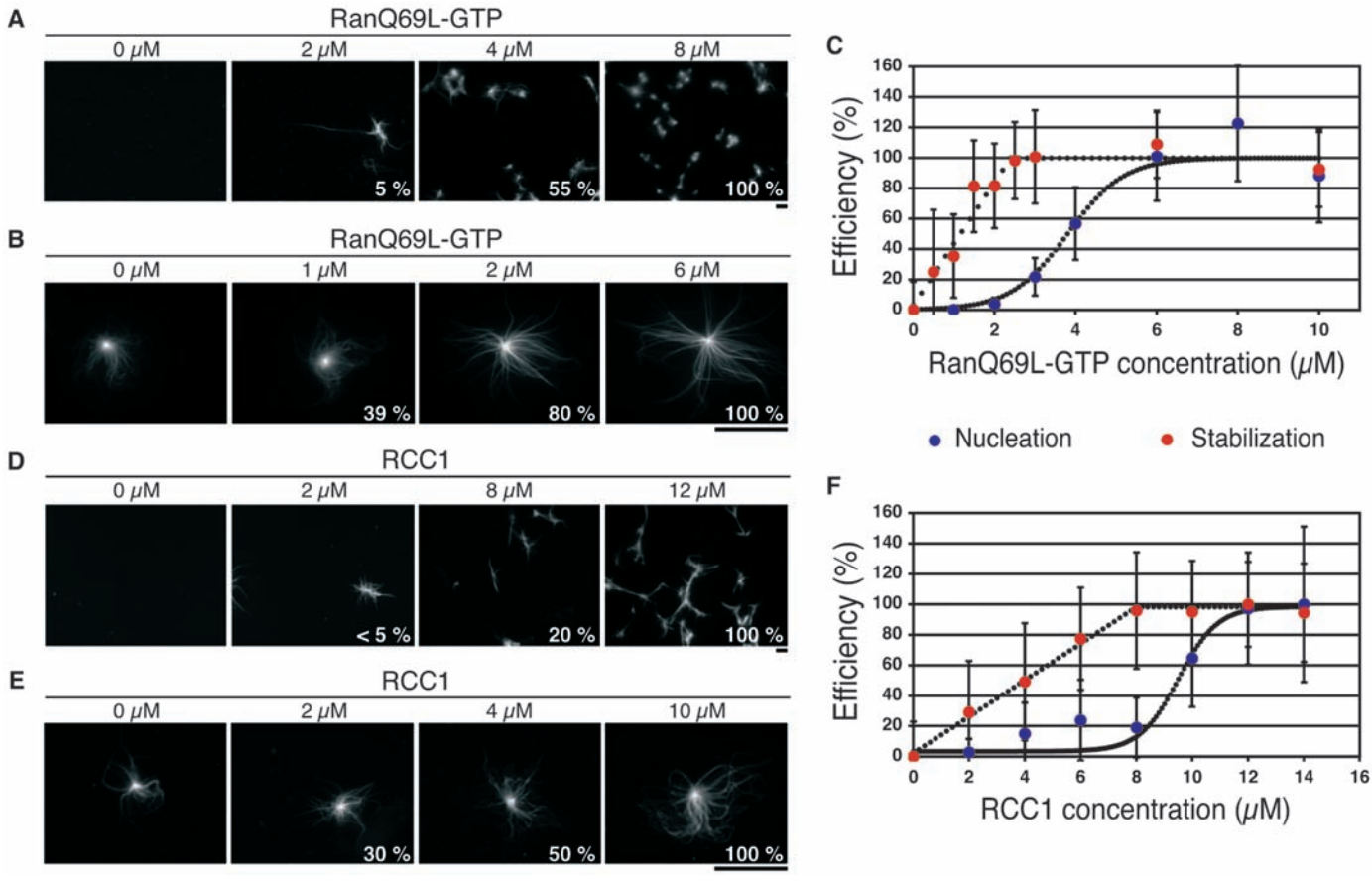

Fig. 2. (**A**) Microtubule nucleation as a function of RanQ69L-GTP concentration. RanQ69L-GTP was added to metaphase extracts containing rhodamine-labeled tubulin (*22*). (**B**) Microtubule stabilization as a function of RanQ69L-GTP concentration. Centrosomes and rhodamine-labeled tubulin were added to extracts together with antibodies against TPX2. (**C**) Microtubule nucleation and stabilization efficiency as a function of RanQ69L-GTP concentration. (**D**) Microtubule nucleation as a function of RCC1 concentration. (**E**) Microtubule stabilization as a function of RCC1 concentration. (**F**) Efficiency of microtubule nucleation and stabilization in response to increasing RCC1 concentrations. Error bars, SD. Scale bars, 10 μm.

(Fig. 1, D and E). The range of a computed spatial lifetime distribution evaluated from the reaction-diffusion theory corresponded well to those reproducibly measured by experiments (Fig. 1, E and F) (*17*). The amplitude variation of their depth (Fig. 1E) is due to the formation of complexes between fluorescent RanGTP and dark endogenous importin-β or other proteins in different experiments, which decreases the dynamic range of the FRET signal.

Because MT nucleation and plus end stabilization occur at different distances from chromosomes (*8*, *9*), such processes could be differentially regulated by the long-range gradient. We therefore quantified MT nucleation and plus end stabilization as a function of global RanGTP concentrations in metaphase *Xenopus* egg extracts and correlated these results with the span of the RanGTP–importin-β complex concentration gradient around chromosomes. RCC1 and a nonhydrolyzable mutant form of RanGTP (in which Gln^{69} is replaced by Leu), RanQ69L-GTP, induce MT nucleation and formation of spontaneous asters in metaphase egg extracts (*12*). We used this assay to quantify MT nucleation in the presence of increasing concentrations of either RCC1 or RanQ69L-GTP (Fig. 2, A and D) (*22*). Half-maximum nucleation efficiency was reached at 4 μM RanQ69L-GTP or 9 μM RCC1 (Fig. 2, C and F). MT nucleation responded in an ultrasensitive manner to the concentration of RanQ69L-GTP and RCC1. To examine the effect of RanGTP concentrations on MT plus end stabilization exclusively, we eliminated the RanGTP-dependent nucleation of MTs by inactivating TPX2 (*23*) and produced asters by adding purified centrosomes that do not require TPX2 to nucleate MTs (Fig. 2, B and E). MT plus end stabilization increased linearly with RanQ69L-GTP or RCC1 concentration up to saturation, reaching half-maximum stabilization efficiency at 1.5 μM RanQ69L-GTP and 4 μM RCC1 (Fig. 2, C and F).

Thus, MT nucleation and plus end stabilization occur at significantly different concentrations of RanGTP, which suggests different spatial regulations of these processes around chromosomes. Using the gradient profiles measured by FLIM around sperm nuclei (Fig. 1E), we could then evaluate the distances at which the gradient of RanGTP–importin-β could affect MT nucleation and plus end stabilization around chromatin (Fig. 3) (*22*). Nucleation should occur in a small region of about 5 ± 5 μm, whereas centrosomal MT plus end stabilization could occur as far as 35 ± 10 μm from chromatin. MT nucleation is restricted to a defined area around chromosomes because of its ultrasensitive response to RanGTP concentration (Fig. 3, C and D), whereas MT plus end stabilization extends over long distances because of its linear response to RanGTP concentration (Fig. 3, A and C).

We next examined whether the formation of a proper bipolar spindle around chromosomes requires the RanGTP–importin-β spatial information gradient. We first added sperm nuclei that contain centrosomes to extracts in which chromosomal MT nucleation had been inhibited by inactivating TPX2 (*22*). This resulted in the formation of aberrant bipolar spindles (*24*, *25*) (Fig. 4A). However, in both control and TPX2-inactivated extracts, 90% of sperm nuclei were connected to centrosomal asters. This shows that chromosomal MT nucleation is not necessary for asymmetric growth of astral MTs and chromosomal capture, but is required for the formation of functional spindles (Fig. 4, B and D). We could now investigate whether a long-range gradient of RanGTP–importin-β was required for the asymmetric growth of MTs toward chromosomes. By varying the concentration of RanGAP and RanBP1 in the extract, we could modulate the reach of the gradient (Fig. 4E) (*17*) and observe the effect on the directional growth of MTs. Decreasing the reach of the gradient by increasing RanGAP and RanBP1 concentrations led to a loss of astral MT asymmetry (Fig. 4A) that was correlated with a strong decrease in the percentage of chromosomes connected to asters (Fig. 4D). Because capture is lost under such conditions, this indicates that a long-range stabilization gradient facilitates biased MT growth and thereby MT capture by chromosomes. A recent theoretical study actually suggests that an unbiased search-and-capture process is unlikely to allow MT capture by chromosomes in a biologically relevant time scale (*26*). However, theory predicts that, in this system, increasing RanGAP and RanBP1 also decreases the amplitude of the RanGTP–importin-β gradient (Fig. 4E) (*17*). This could affect chromosomal capture of MT plus ends simply by lowering the concentration of free NLS-proteins. Therefore, we investigated whether increasing the concentration of free NLS-

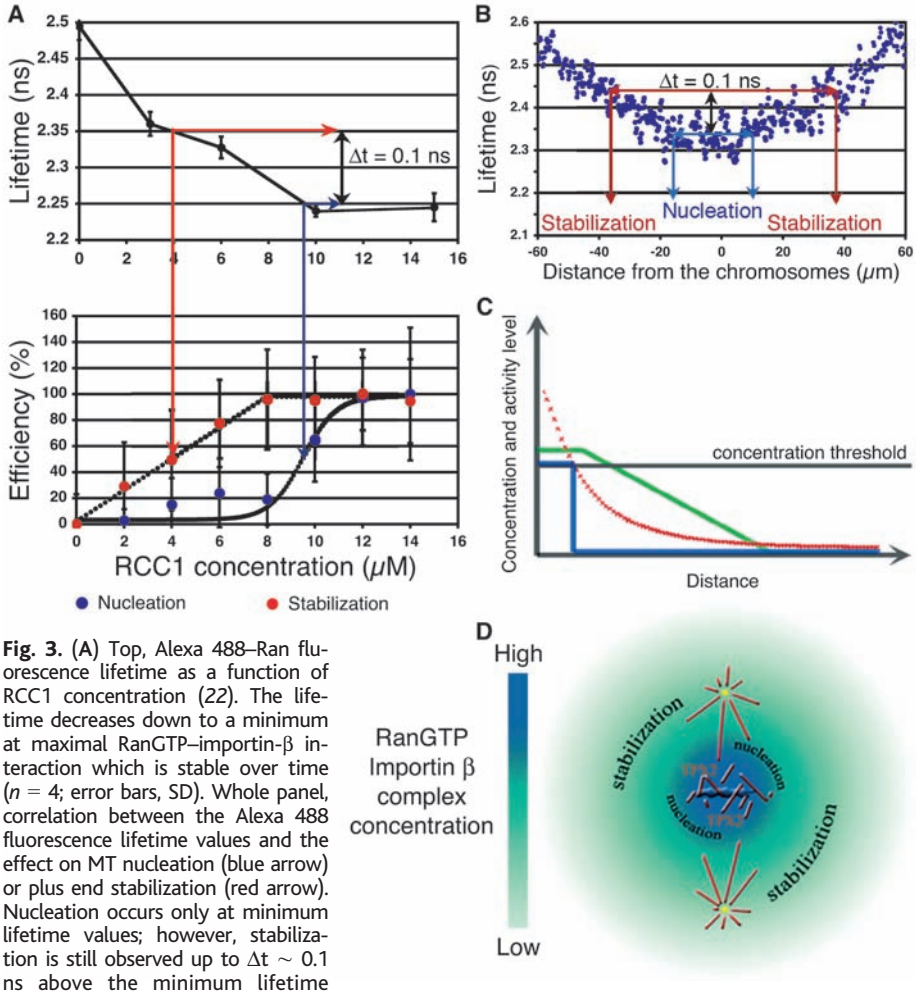

Fig. 3. (**A**) Top, Alexa 488–Ran fluorescence lifetime as a function of RCC1 concentration (*22*). The lifetime decreases down to a minimum at maximal RanGTP–importin-β interaction which is stable over time (n = 4; error bars, SD). Whole panel, correlation between the Alexa 488 fluorescence lifetime values and the effect on MT nucleation (blue arrow) or plus end stabilization (red arrow). Nucleation occurs only at minimum lifetime values; however, stabilization is still observed up to Δt ~ 0.1 ns above the minimum lifetime value. (**B**) Determination of the microtubule nucleation (blue arrows) and stabilization (red arrows) regions around sperm nuclei using an experimental gradient profile (blue dotted curve). (**C**) Differential spatial effects of the RanGTP–importin-β concentration gradient (crossed red line) on microtubule nucleation (blue) and stabilization (green). (**D**) Top view of the effect of the RanGTP–importin-β concentration gradient on microtubule nucleation via TPX2 and plus end stabilization of astral microtubules. Microtubules, red; chromosomes, blue; centrosomes, yellow.

proteins globally in the cytoplasm is sufficient to form a spindle. This was done by increasing RCC1 concentration in the extract, which flattened the gradient (Fig. 4E) (*17*). This resulted in a disorientation of MT growth relative to chromosomes, a loss of bipolar spindle assembly, the formation of random MT structures (Fig. 4C) (*17*), and a strong decrease in MT-chromosome connections (Fig. 4D) (*12*). These experiments show that concentration gradients of active MT regulators must operate within well-defined dimensions to achieve proper spatial coordination of spindle assembly (Fig. 3, C and D).

This study shows that chromosomes create a local perturbation in the homogeneous mitotic cytoplasm that generates a radial symmetry. Further breakdown of this radial symmetry by the self-organization of microtubules and their motors (*27*) results in the establishment of a bilateral symmetry centered on chromosomes. Thus, the Ran system does more than simply signal where the chromosomes are; by interfering with the symmetry properties of the mitotic cytoplasm, it functions as a control element that spatially coordinates the self-organization of the MT-chromosome system.

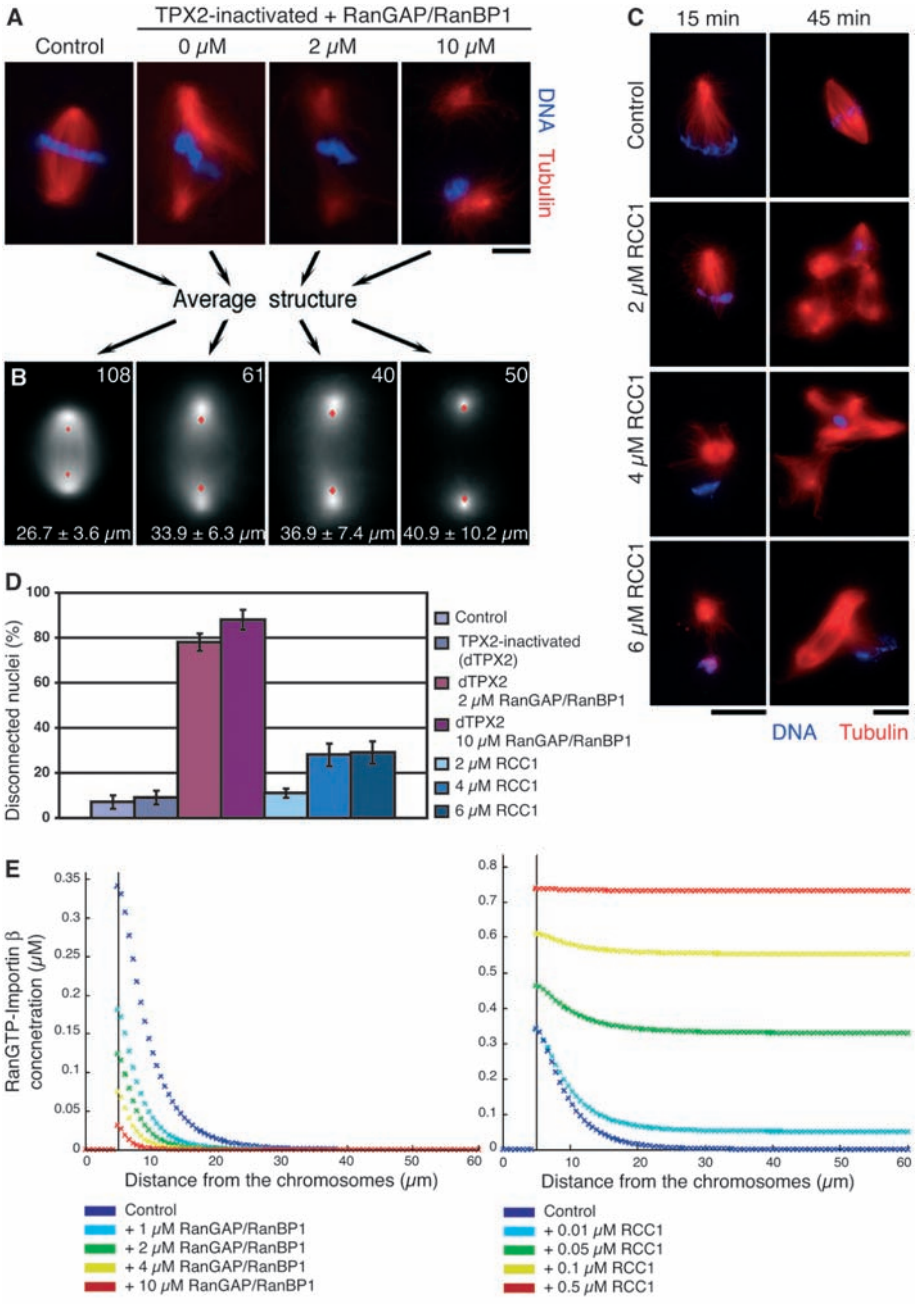

Fig. 4. (**A**) Spindle assembly around sperm nuclei added to M-phase extracts form bipolar spindles (control lane), except in the presence of TPX2 antibody (*22*), and further addition of RanGAP and RanBP1. Scale bar, 10 μm. (**B**) Average microtubule density calculated out of the structures acquired in (A). The asymmetry of centrosomal asters is lost when the microtubule density center of mass (red dots) colocalizes with the centrosomes at the poles of the structures (*21*). Number of structures used and average size ± SD are indicated. (**C**) Perturbation of spindle assembly by increasing RCC1 concentration. Sperm nuclei containing centrosomes added to M-phase extracts produce asymmetric asters after 15 min (*22*). This asymmetry is progressively lost with increasing RCC1 concentrations. After 45 min, sperm nuclei form bipolar spindles (control lane) except in samples containing increasing amounts of RCC1, where disorganized structures are observed. Scale bars, 15 μm. (**D**) Percentage of chromosomes disconnected from centrosomal asters in the samples observed in (A) and in (C) (*22*). Error bars, SD. (**E**) Calculated spatial distribution of RanGTP–importin-β concentration in the presence of increasing amounts of RanGAP and RanBP1 (left) or RCC1 (right). Vertical black line, interface between chromatin (left side) and cytoplasm (right side).

References and Notes

1. M. Kirschner, T. Mitchison, *Cell* **45**, 329 (1986).
2. E. A. Smirnova, A. S. Bajer, *Cell Motil. Cytoskeleton* **40**, 22 (1998).
3. W. Steffen, H. Fuge, P. Dietz, M. Bastmeyer, G. Müller, *J. Cell Biol.* **102**, 1679 (1986).
4. H. Matthies, H. McDonald, L. Goldstein, W. Theurkauf, *J. Cell Biol.* **134**, 455 (1996).
5. E. Karsenti, J. Newport, M. Kirschner, *J. Cell Biol.* **99**, 47s (1984).
6. A. A. Hyman, E. Karsenti, *Cell* **84**, 401 (1996).
7. E. Karsenti, I. Vernos, *Science* **294**, 543 (2001).
8. R. Heald *et al.*, *Nature* **382**, 420 (1996).
9. R. E. Carazo-Salas, E. Karsenti, *Curr. Biol.* **13**, 1728 (2003).
10. P. Kalab, R. T. Pu, M. Dasso, *Curr. Biol.* **9**, 481 (1999).
11. A. Wilde, Y. Zheng, *Science* **284**, 1359 (1999).
12. R. E. Carazo-Salas *et al.*, *Nature* **400**, 178 (1999).
13. D. Gorlich, U. Kutay, *Annu. Rev. Cell Dev. Biol.* **15**, 607 (1999).
14. H. Y. Li, Y. Zheng, *Cell Cycle* **3**, 993 (2004).
15. P. Kalab, K. Weis, R. Heald, *Science* **295**, 2452 (2002).
16. M. Dogterom, M. A. Felix, C. C. Guet, S. Leibler, *J. Cell Biol.* **133**, 125 (1996).
17. Supporting text is available on *Science* Online.
18. M. Floer, G. Blobel, *J. Biol. Chem.* **271**, 5313 (1996).
19. M. Floer, G. Blobel, M. Rexach, *J. Biol. Chem.* **272**, 19538 (1997).
20. F. R. Bischoff, D. Gorlich, *FEBS Lett.* **419**, 249 (1997).
21. F. S. Wouters, P. J. Verveer, P. I. Bastiaens, *Trends Cell Biol.* **11**, 203 (2001).
22. Materials and methods are available as supporting online material on *Science* Online.
23. O. J. Gruss *et al.*, *Cell* **104**, 83 (2001).
24. T. Wittmann, M. Wilm, E. Karsenti, I. Vernos, *J. Cell. Biol.* **149**, 1405 (2000).
25. O. J. Gruss *et al.*, *Nat. Cell Biol.* **4**, 871 (2002).
26. R. Wollman *et al.*, *Curr. Biol.* **15**, 828 (2005).
27. F. Nedelec, T. Surrey, E. Karsenti, *Curr. Opin. Cell Biol.* **15**, 118 (2003).

28. We thank F. Nedelec for writing the Matlab macros used for spindle and aster analysis and for his help regarding the development of the reaction-diffusion model. We also thank C. Tischer, who suggested the time integration for the reaction-diffusion system; P. Verveer and T. Squire for their help with FLIM acquisition and data analysis; I. Mattaj for continual discussions; and O. Gruss for help with the preparation of recombinant proteins.

Supporting Online Material

www.sciencemag.org/cgi/content/full/309/5739/1373/DC1
Materials and Methods
SOM Text
Figs. S1 to S12
Tables S1 to S4
References and Notes

10 June 2005; accepted 15 July 2005
10.1126/science.1115964